Energy Advances

Accepted Manuscript

This article can be cited before page numbers have been issued, to do this please use: J. T. B. Maldifassi, J. B. Russell, J. Kim, E. Brightman, X. Chen and D. Bae, *Energy Adv.*, 2024, DOI: 10.1039/D4YA00368C.

ROYAL SOCIETY OF CHEMISTRY

rsc.li/energy-advances

View Article Online
DOI: 10.1039/D4YA00368C

ARTICLE

Evaluation of redox pairs for low-grade heat energy harvesting with thermally regenerative cycle

Received 00th January 20xx,
Accepted 00th January 20xx

DOI: 10.1039/x0xx00000x

José Tomás Bórquez Maldifassi,[a,†] Joseph B. Russell,[b,†] Jungmyung Kim,[b] Edward Brightman,[c] Xiangjie Chen,[b] Dowon Bae[a,b]*

Waste heat, particularly low-grade (lower than 100°C), represents a considerable amount of energy loss across different industries and areas of human development. In recent years, different ways of harvesting heat have been the focus of extensive research, with the thermally regenerative electrochemical cycle (TREC) being of particular interest due to its promising results, derived from using the temperature coefficient of electrolytes to obtain more efficient charging and discharging battery cycles. While studies have shown groundbreaking results by trial-and-error-based combinations of different redox couples, these studies have been mostly isolated from one another, possibly missing unseen potentials of unexplored redox couple combinations. Therefore, a wider view of these combinations is explored in this work to screen them for the TREC battery applications. Herein, we present a comprehensive survey of the redox couples used in the literature to highlight the untapped potential of the TREC cell. Furthermore, strategic guidelines on choosing the efficient redox couples for the TREC with engineering remarks and insights for their practical heat-to-electricity conversion applications.

1 Introduction

It has been estimated that 72% of worldwide primary energy is lost while converting to useful energy and over 60% of this can be categorised as low-grade heat (<100°C).[1] Therefore, the rational utilisation of low-grade heat is one of the most promising sources with great potential to solve current energy challenges. However, converting low-grade heat using a conventional solid-state thermoelectric device-based system is challenging due to their low conversion efficiencies (~2-7%) attributed to their modest Seebeck values (~0.2mV/K)[2] and poor cost-effectiveness (~22 £/W).[3] Meanwhile, the aqueous thermogalvanic cell with a thermally regenerative electrochemical cycle (TREC) is known to have high cost-effectiveness (~0.4 £/W)[4] as their thermogalvanic coefficients are around one order of magnitude higher than static devices, making them more applicable in low-grade heat scenarios. Moreover, it has been reported that when combined with photovoltaic cells the thermal damage of the photovoltaic cells can be remedied by heat diffusion (i.e., heat-sink).[5,6] Recent reports have demonstrated that thermogalvanic TREC cells have a heat-to-electricity conversion efficiency of close to 6% at the laboratory level.[3,7] Notwithstanding these advantages, thermogalvanic cells are still in the stage of continuing exploration to find appropriate combinations of redox couples, which can exhibit high-temperature sensitivity (i.e., thermogalvanic (Seebeck) coefficient).

For the last few years, intensive effort has gone into achieving a large thermogalvanic coefficient cell. Wang et al. claimed in their report that their thermoelectrochemical cell with a 3.52 % efficiency using a combination of NiHCF||Ag/AgCl (−0.74 mV/K). [8] Lee et al. demonstrated the record TREC efficiency of 5.7% with $Cu^{0/2+}$||CuHCF combination, showing a thermogalvanic coefficient of -1.2 mV/K.[9,10] Chun et al. demonstrated a high coefficient TREC cell (-2.27 mV/K) using a NiHCF||$[Zn(NH3)]_4^{2+}$/Zn^{2+}.[9] A TREC cell using a conventional vanadium redox flow battery (RFB) demonstrated by Reynard et al. can be considered as monumental work that attempted to introduce the TREC concept to vanadium RFBs for the first time.[11] It showed 2.6% heat-to-electricity conversion efficiency with a coefficient of -1.16 mV/K. However, due to the nature of the vanadium (VO_2^+/VO^{2+} or $V^{5+/4+}$), precipitation formation would challenge long-term operations at elevated temperatures.[11]

Among various redox couples frequently used for aqueous electrochemical cells, the largest thermogalvanic coefficient have been observed in I_3^-/I^- redox couples, which varies between 0.9-4.2 mV/K depending on the type of additives.[12] Br_2/Br^- redox couple varies between 0.5-3 mV/K,[13] and ferro/ferri-cyanide ($Fe(CN)_6^{3-}$/$Fe(CN)_6^{4-}$) is reported to have a moderate negative value of −1.42 mV/K.[14]

Though the TREC cell is still at a very early stage of research based on trial-and-error screening of chemicals, the studies mentioned above clearly imply the great prospect of the TREC-

[a]Institute of Mechanical, Process and Energy Engineering (IMPEE), School of Engineering and Physical Sciences, Heriot-Watt University, Edinburgh EH14 4AS, United Kingdom
[b]Wolfson School of Mechanical, Electrical and Manufacturing Engineering, Loughborough University, Loughborough LE11 3TU, United Kingdom
[c]Department of Chemical and Process Engineering, University of Strathclyde, Glasgow G1 1XL, United Kingdom
† Footnotes relating to the title and/or authors should appear here.
Electronic Supplementary Information (ESI) available: [details of any supplementary information available should be included here]. See DOI: 10.1039/x0xx00000x

based technology for efficient heat-to-electricity conversion. Herein, we conduct a meticulous study of the reported TREC cells to present a comprehensive re-assessment and screening of previously used redox couples for TREC and similar thermogalvanic cells to provide a short list of recombined redox couple combinations that can untap the potential of the TREC cell as a promising heat-to-electricity conversion and storage technology.

2 Working principles of TREC redox cells

TREC is a cyclical process in which electrical work is generated by charging and discharging an electrochemical cell at different temperatures[15]. Such systems can be likened to thermomechanical engines, which are theoretically limited by the Carnot efficiency. In practice, the energy recuperation effectiveness is dependent on the cell chemistry, the system's ability to manage heat transfer and the electrical performance of the cell(s)[10]. The overall heat-to-electricity conversion, which reflects the electrical work recovered against the total heat applied to a single cell system, can be expressed as:[2,6]

$$\eta = \frac{W_{net}}{|\alpha_{cell}|T_D Q_C + (1-\eta_{HR})C_p \Delta T} \quad (1)$$

Where $\mathbf{W_{net}}$ is the net work recovered from the cycle, $\boldsymbol{\alpha_{cell}}$ is the overall thermoelectric coefficient (mV/K), which is paired with the discharge temperature $\boldsymbol{T_D}$ (K) and the charge capacity $\boldsymbol{Q_C}$ to account for heat absorbed by the heat collector or electrolyte at high temperatures, which cannot be recovered. $\boldsymbol{\eta_R}$ is the heat exchange efficiency, which reflects how much heat is retained between cycles. This is paired with the heat capacity $\boldsymbol{C_p}$ and temperature change $\boldsymbol{\Delta T}$ to account for energy lost when heating up the remainder of the system. Note that this general heat-to-electricity conversion efficiency (eq. 1) only accounts for the efficiency of the generated energy and does not account for the energy supplied to charge the cell. In the case of flow-based technologies, such as TREC with redox flow batteries, we suggest referring to formulas with a flow rate factor elsewhere.[3] As TREC is in an early research stage, various types of technologies are reported in the literature. The self-charging single cell by Yang et al. and the dual flow cell system by Bleeker,[4,16] neutralisation flow cell by Loktionov,[17] the TREC system based on the Brayton cycle by Rajan[18] and Chen,[19] are good examples of this diversity.

Electrolyte design plays a crucial part in TREC performance as it will determine the $\boldsymbol{\alpha_{cell}}$, $\boldsymbol{Q_C}$ and $\boldsymbol{C_p}$ values. Additionally, improvements in the charge-transfer kinetics of reported electrolyte pairs have been commended for improving the viability of TREC systems by further overcoming electrical losses.[2] Electrolyte optimisation is a multi-factor aspect, but the scope of this work concerns only the thermal coefficient, redox potential, pH range, and solubility, which are the most critical properties of TREC performance and its system reliability. For a half-cell reaction (either oxidation or reduction reaction), the thermogalvanic coefficient α can be expressed simply as:[20]

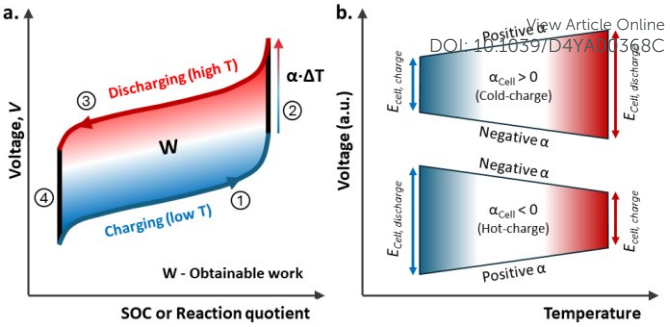

Fig. 1 (a) Voltage-SOC diagram of TREC for $\alpha_{Cell} > 0$ with its sequence of operation (#1 to #4) and (b) open circuit voltage shifts by electrolyte temperature change for both positive (upper) and negative α_{Cell} cases (lower).

$$\boldsymbol{\alpha} = \frac{\partial \boldsymbol{E}}{\partial \boldsymbol{T}} = \frac{\Delta \boldsymbol{S}}{\boldsymbol{nF}} \quad (2)$$

where E is the redox potential of the redox couple, F is Faraday's constant, ΔS is the entropy change, and n is the stoichiometric number of electrons involved in the reaction. For a full-cell reaction consisting of two half-reactions, the thermoelectric coefficient becomes the difference between the two half cells:[10,11]

$$\boldsymbol{\alpha_{Cell}} = \boldsymbol{\alpha_+} - \boldsymbol{\alpha_-} \quad (3)$$

where α_+ and α_- are thermogalvanic coefficients for anodic (positive) and cathodic (negative) sides, respectively. Similarly, the standard cell voltage at 25°C, E^0_{cell}, corresponds to the difference in standard redox potential of both half cells:

$$E^0_{Cell} = E^0_+ - E^0_- \quad (4)$$

The cell voltage as a function of its temperature change (i.e., $T_{high} - T_{low}$) can be calculated using the following equation:

$$E_{Cell}(T) = E^0_{Cell} + \alpha_{Cell}\Delta T \quad (5)$$

Under an assumption of fully solubilised electrolyte condition with a 1:1 stoichiometric reaction, the cell voltage also can be described by the following form of the Nernst Equation:[4]

$$E_{Cell} = E_{Cell}(T) - \frac{RT}{nF}\ln Q = \left(E^0_{Cell} + \alpha_{Cell}(T_{high} - T_{low})\right) - \frac{RT}{nF}\ln\frac{SOC^2}{(1-SOC)^2} \quad (6)$$

where R is the universal gas constant, and Q is the reaction quotient reflecting the molar fraction of the redox species during the charging/discharging process. This corresponds to the state-of-charge (SOC) of the battery system.

The heat-to-electricity conversion in the TREC occurs from the shift in cell voltage due to the change in operating temperature, where cells are charged and discharged at different temperatures to capitalise on this change in potential. In the redox flow battery case, this can be reservoir temperatures. A voltage-SOC diagram of the TREC for a positive α_{Cell} in Figure 1a clearly demonstrates the overall heat-to-electricity conversion process described above.

It is worth noting that the cell voltage change can be maximised by combining redox electrolytes with opposite α values. For instance, a positive α electrolyte in one half-cell and a negative in the complimentary half-cell. The sign of the thermal coefficient of the cell depends on the standard redox potentials and the sign of the temperature coefficients of the selected

View Article Online
DOI: 10.1039/D4YA00368C

redox couples. As shown in Figure 1b, α_{CellI} can either increase or decrease as temperature rises. Naturally, in the case of negative α_{CellI}, the TREC cell should be charged at a high temperature and discharged at a low temperature to generate energy, W, from the heat-to-electricity conversion.

It must be noted that α_{CellI} is not entirely dependent on the redox pairs, and can be related to the additives, hydration structure, etc. For instance, adding guanidium and urea to $Fe(CN)_6^{3-/4-}$ electrolyte can improve its thermogalvanic coefficient up to 4.2 mV/K.[21] The addition of the poly(4-styrenesulfoic acid) as an intercalating cation for the CuHCF is also known to increase the reaction entropy.[22] Also, increased disruption of solvation structures and hydrogen bonds by introducing chaotropic ions may allow molecules to further disperse after a redox reaction occurs.[23] In this study, we explore various types of redox ions based on their standard properties, and therefore addressing hydration structure and other molecular interaction properties is beyond the scope of this work.

3 Selection criteria

The wide range of existing redox reactions leads to an enormous theoretical number of possible redox couple combinations (catholyte/anolyte pairs). Naturally, excellent computational and experimental databases of the redox couples for conventional redox battery applications do exist.[24–26] However, such databases have not yet included the additional evaluation criteria of thermogalvanic properties. The TREC research so far has relied on trial-and-error selection of redox couples. The operational feasibility of TREC batteries is also highly dependent on the choice of their redox couples. Recent work by Bleeker et al.[4] effectively described the basic selection criteria for efficient and reliable TREC redox cells with a low-grade heat source. In addition to these standards introduced ref. [3], the criteria used in this work are listed as follows:

1. To generate useful amounts of energy, the difference in the thermogalvanic coefficient (i.e., Seebeck coefficient) of both half cells (i.e., catholyte and anolyte sides) must be significantly high. The absolute value is important regardless of whether it is positive or negative.
2. Redox species are required to behave in a stable manner in the range of low-grade heat. Phenomena such as precipitation formation or unwanted side reactions at elevated temperatures should not be observed.
3. Redox species involved in each half-cell are required to have the same valence sign to allow for effective separation with a monopolar ion exchange membrane.[4] Bipolar membranes could work for cases with different valence signs (e.g., $Fe(CN)_6^{3-/4-}||Zn^{0/2+}$), but the current performance of these membranes can lead to large energy losses (e.g., high ionic voltage losses) as demonstrated elsewhere.[27]

While addressing most of the relevant aspects of the redox couple selection for conventional redox batteries, additional selection criteria were added to narrow down further the number of redox couples deemed most efficient for TREC redox batteries:

4. To avoid any undesired chemical crossovers through the membrane, both catholyte and anolyte sides must contain redox species and supporting electrolytes which remain stable at the same pH levels for their stability and proper functioning. This is again related to the use of monopolar membranes mentioned above. Bipolar membranes can maintain a pH difference between the catholyte and anolyte sides.
5. Since the redox couples need to react in an aqueous environment with feasible reversibility, redox reactions should take place either within the electrolyte or between the ions in the electrolyte and the solid electrode (e.g., $Cu^{0/2+}$ and $Zn^{0/2+}$). The aqueous electrolyte was chosen as the solvent of the redox couples in this study, considering the general thermally regenerative redox cell studies reviewed in this work. Water has a wide versatility, such as relatively low cost, safe operating range under low-grade heat, and appropriate viscosity suitable to ordinary flow cell systems.

Table 1 Specifications and performance metrics from the literature.

Couple	Thermal Coefficient, α [mV/K]	Standard Redox Potential, E^0 [V]	Solubility M [M]	Stable pH range	
				Lower	Higher
$Fe^{2+/3+}$	1.76 [14]	0.68 [14]	1.3 [14]	0 [28]	1.5 [28]
$Fe(CN)_6^{3-/4-}$	-1.42 [14]	0.47 [14]	0.4 [14]	8.5[29]	10.5 [29]
I_3^-/I^-	1.04 [4]	0.66 [30]	1.0 [4]	6 [31]	9.5 [31]
Br_2/Br^-	2.30 [32]	1.19 [33]	0.2 [34]	0 [35]	14 [35]
$Zn^{0/2+}$	0.40 [36]	-0.80 [33]	14.67 [37]	0[38]	8.5 [38]
Ag^{1+}/AgCl	0.25 [8]	0.42	4.76*[39]	0 [40]	12.5 [40]
$Cu^{0/2+}$	-0.30 [41]	0.29 [42]	3.5 [41,43]	0 [40]	6 [40]
$Cu^0/Cu(NH_3)_4^{2+}$	-1.00 [41]	0.15 [44]	N/A	11 [43]	14 [43]
$V^{2+/3+}$	1.01 [11]	-0.29 [45]	1 [11]	0[46]	1.8 [46]
$V^{4+/5+}$	-0.15 [11]	1.21 [45]	1 [11]	0 [46]	3 [46]
NiHCF*	-0.88 [9]	0.73 [9]	4.76*[39]	2 [8]	2 [8]
$Zn^0/Zn(NH_3)_4^{2+}$	1.40 [9]	-1.04 [47]	N/A	0 [38]	8.5 [38]
CoHCF*	0.89 [48]	0.78 [48]	4.76*[49]	N/A	N/A
CuHCF*	-0.36 [10]	1.16 [50]	10.38*[49]	N/A	N/A
$Na^{0/1+}$	0.73 [51]	0.28 [47]	14.8 [49]	N/A	N/A
$Li^{0/1+}$	0.88 [51]	0.49 [52]	7.8 [49]	N/A	N/A

*Solubility for these specific couples depends on the chemical substance that is released and absorbed into the electrolyte as the charging/discharging cycle occurs. For NiHCF, CoHCF, and AgCl, the chemical corresponds to KCl. For CuHCF, the chemical corresponds to $NaNO_3$. Detail chemical reactions for these metal hexacyanoferrates can be found in ESI.† For Zn^{2+}, it corresponds to $ZnCl_2$.

View Article Online
DOI: 10.1039/D4YA00736G

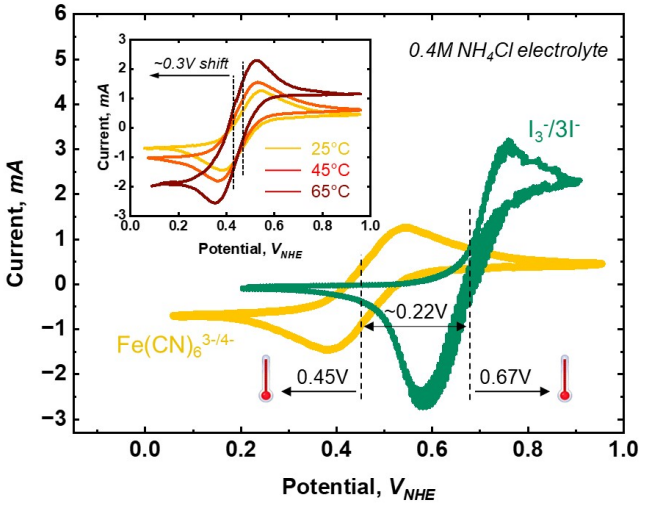

Fig. 2 Example cyclic voltammetry (CV) curves of 0.4M solutions of $Fe(CN)_6^{3-/4-}$(yellow) and $I_3^-/3I^-$ redox couples (green) in 0.4M NH4Cl electrolyte using a scan rate of 20 mV sec^{-1}. The inset shows CV profiles for the $Fe(CN)_6^{3-/4-}$ redox couples measured at different temperatures. The E^0_{cell} can be defined as the difference between the standard reduction potentials of the oxidation and reduction half-reactions from the measured CVs. The figure above represents the case of a positive α_{cell} under a temperature change.

Redox couples used in previous TREC batteries and other similar thermally regenerative electrochemical cells were selected according to the criteria listed above, and only combinations that met these conditions would undergo further evaluation. We note that, despite the detailed criteria listed above, this study's limitation is that ohmic, concentration, and activation overpotentials were not considered.

4. Literature data acquisition

A thorough study was conducted based on recent experimental investigations on both flow and static type TRECs and their summarised properties are listed in Table 1. Along with these thermally regenerative redox cell studies, complementary property data was also acquired for the individual redox couples, including standard redox potential, solubility, and stable pH window.

For a valid and fair comparison, the standard redox potential (E^0) can be defined as the difference between the standard reduction potentials of the oxidation and reduction half-reactions under standard conditions (i.e., 25°C, 1 atm, and 1M) (see Fig. 2). The maximum solubility limit of the TREC system is defined by the half-reaction with the lowest solubility value, as this infers the maximum number of transferrable charges for both electrodes. In the case of the stable pH range of the redox couples, values were obtained either by analysing the Pourbaix diagram of the elements or from previously reported experimental values.

Table 1 displays the values for thermal coefficient, standard redox potential, solubility and pH stability range obtained for the various redox chemicals used in previous TREC studies. It is worth mentioning that couples, such as $Fe^{2+/3+}$, $Fe(CN)_6^{3-/4-}$, Br_2/Br^-, and $Zn(NH_3)_4^{2+}/Zn$ show particularly high values for thermal coefficient (-1.42, 2.40, and 1.40 mV/K, respectively). Among them, the Br_2/Br- redox couple is a complex case. Thermo-cells with values as high as 5.68 mV/K have been reported,[13,53] but these values are found under conditions that interfere with the previously described selection criterion number 2. Instead, a more realistic value of 2.3 mV/K, as found by Endo et al.[32] under a stable reaction condition, is used in this study.

While marked as insoluble, $Ag^{0/1+}$, CuHCF, CoHCF and NiHCF can still be used as viable redox couples in the TREC mechanism by being present as the main component of the metallic electrodes rather than exclusively dissolved in the electrolyte solutions. It is important to note that solubilities of $Ag^{0/1+}$,[8] NiHCF,[9,54] CoHCF,[48] and CuHCF[6,10] correspond to specific ions released into the electrolytes in this survey: Cl- for Ag^+/AgCl, K^+ for NiHCF and CoHCF, and Na^+ for CuHCF. Also, we note that Li^+, Ru^+ and other mixed cations can be intercalated with metal hexacyanoferrates as demonstrated elsewhere.[55,56] Additionally, solubilities for copper ammonia and zinc ammonia are not readily available. In the $Li^{0/1+}$ and $Na^{0/1+}$ cases, Li^+ and Na^+ ions were dissolved in the $LiClO_4$ and $NaClO_4$ electrolytes, respectively,[51] and the relevant pH stability ranges were also not clearly demonstrated. Concerning the polyiodide couple, while the solubility is usually in the range of 0.1~0.3 M,[18,57] recent redox flow battery research has reported values well above 1 M using ZnI and LiI salts,[4,58] which made this value more fitting for this specific research.

5 Screening results and discussion

A matrix in Fig. 3 summarises the results for combinations of redox couples listed in Table 1. Overall, more than 80 variants are combined, showing the expected relevant properties. These combinations give the theoretical result of how a TREC would work if it were to use the two involved chemicals as its redox active species.

Note that combinations for the cations and anions are displayed separately to make them have the same valence sign (refer to criterion #3 in chapter 3). Information that was unable to be retrieved is marked as N/A. In cases where there is no overlapping pH range between two selected redox couples, they are marked as N.C. (non-compatible).

On the upper x-axis, the studied redox couples are arranged by standard redox potential, E^0, in a descending manner (left to right). The number on the top right of the redox couples in the information box indicates the number of participating electrons in each redox reaction. The intersection of couples displays the theoretical thermal coefficient value of the cell consisting of the chosen redox couples, the maximum solubility limited by the lower value of both redox couples, and the pH range in which both couples can remain stable.

Impractical combinations have been coloured in light red on the figures. Particularly, combinations with $V^{4+/5+}$ redox couple are invalid selections since solid vanadium pentoxide (V_2O_5) precipitation is formed above temperatures over 60°C,[11,11] violating the above criterion #2. The Br_2/Br^- redox couple, while displaying a high thermal coefficient, is invalid due to a similar issue: a low boiling point of 59°C with a high vapour pressure,[4] which can damage the cell and tubing. The combinations of the

View Article Online
DOI: 10.1039/D4EA00388C

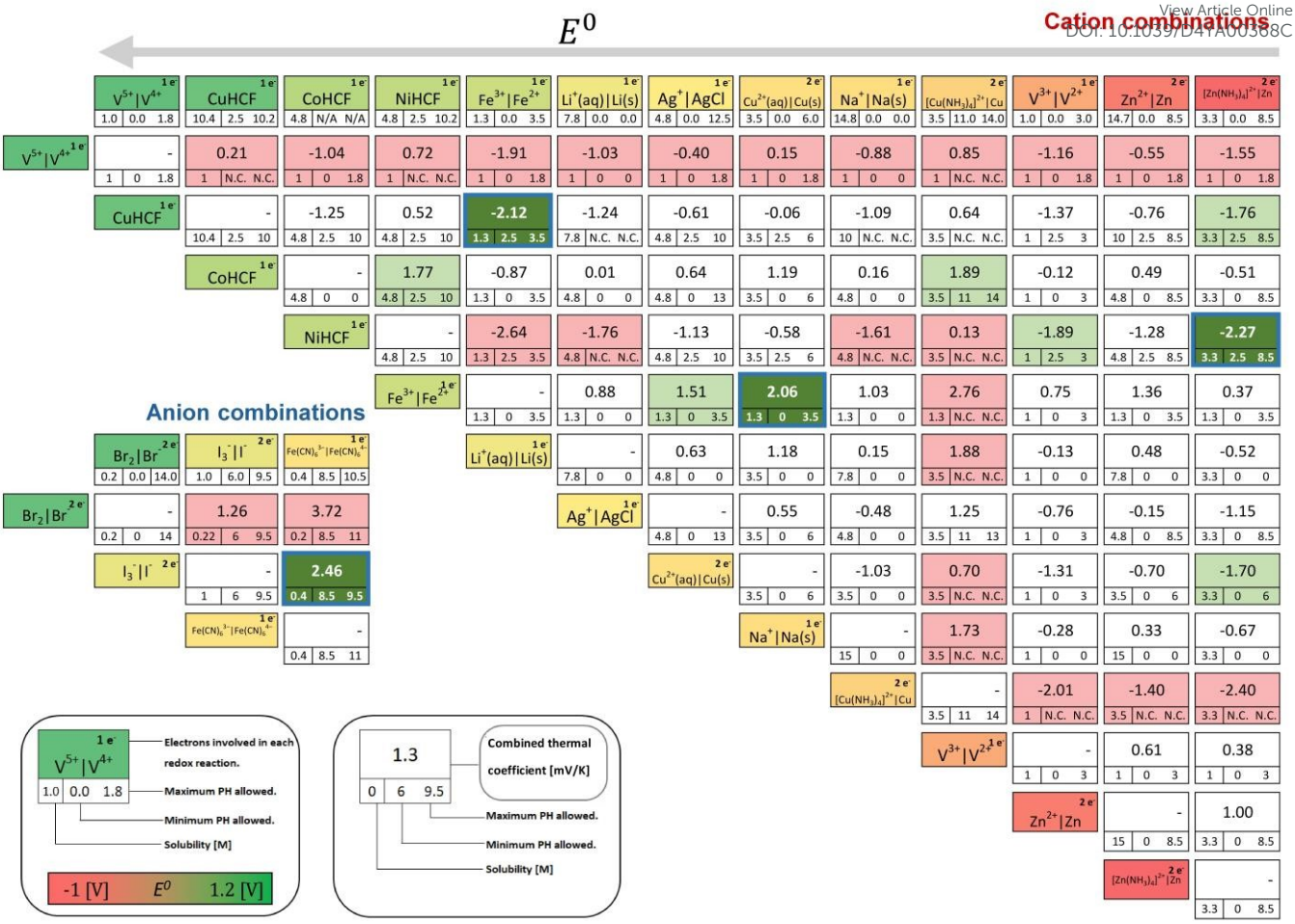

Fig. 3 This redox couple mixture matrix summarises expected cell characteristics, including the cell voltages, thermogalvanic coefficients of the cell, solubilities, and their operatable pH ranges. Overall, 78 and 3 combinations for cations and anions redox couples, respectively, are evaluated in this matrix.

redox couples that cannot satisfy the selection criterion #4 (stable pH range) are also marked with red. A representative case is $Fe^{2+/3+}||Cu(NH_3)_4^{2+}/Cu^0$, which is expected to show the highest value of α_{Cell} (2.76 mV/K) among cation combinations in Figure 3. The $Zn(NH_3)_4^{2+}/Zn^0||Cu(NH_3)_4^{2+}/Cu^0$ shows a similar situation. In both cases, compromising the stable pH range for $Cu(NH_3)_4^{2+}$ could jeopardise the solubility required for Cupric ions Cu^{2+} to combine with the NH_3 molecules in the solution successfully.[43]

Ultimately, the combinations that satisfy all the selection criteria described in Chapter 3 are marked in green. Of these potential candidates, the four best combinations according to criteria described earlier have been highlighted with a blue outline identifier: $[Zn(NH_3)_4]^{2+}/Zn^0||$NiHCF, $Fe^{2+/3+}||$CuCHF, and $Fe^{2+/3+}||Cu^{0/2+}$ as the highest α_{cell} combinations among the cation matrix, and $I_3^-/I^-||Fe(CN)_6^{3-/4-}$ from the anions available. Further analysis, its advantages, limitations, and their voltage-charge behaviours will be discussed below.

$Fe(CN)_6^{3-/4-}||I_3^-/I^-$ The hexacyanoferrate and iodide/polyiodide combination has the largest thermal coefficient of 2.5 mV/K. However, it shows a narrow, stable pH range between 8.5 and 9.5. Moreover, it has a low solubility of 0.4 M (limited by the low solubility of hexacyanoferrate in water). As a direct consequence, a large reservoir of electrolytes would be required to guarantee sufficient energy storage. The single electron charge operation, as well as the low solubility limit, causes this pair to have the lowest charge density, meaning it has the lowest estimated conversion efficiency of all the pairs considered despite having the highest alpha value. Another issue with this combination is the low cell voltage (0.19V at RT), implying that many stacked cells would be required to generate useful amounts of energy.[13]

This specific combination[4] was demonstrated in a conventional thermogalvanic cell configuration, where each electrolyte is operated at a different temperature rather than subjecting the whole system to the same temperature change.

To predict charging/discharging behaviour in the TREC regime for the selected redox couple combination, a theoretical scenario at two different temperatures (i.e., T_{low} = 25°C and T_{high} = 80°C) has been established. Fig. 4 depicts Nernst behaviours at two different temperature conditions with the voltage as a function of the state of charge of the cell using eq. 6.

$Fe^{2+/3+}||Cu^{2+/0}$ The Iron and Copper redox combination also shows promising values. It satisfies the basic selection criteria with a combined thermal coefficient of 2.06 mV/K and a

View Article Online
DOI: 10.1039/D4YA00368C

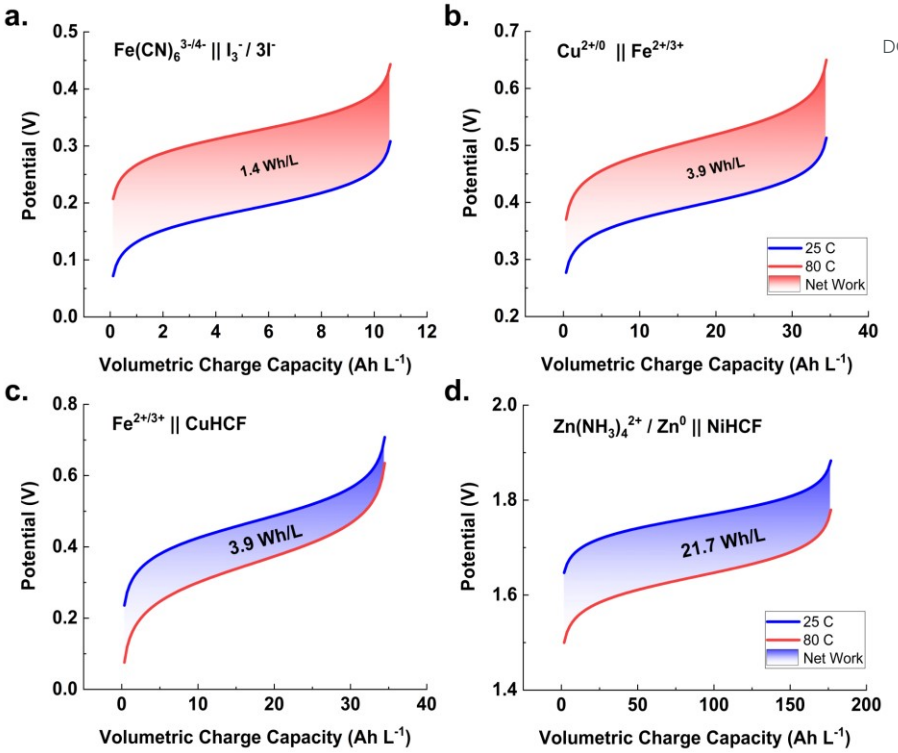

Fig. 4 Cell voltage vs. charge capacity plot of the TREC cycle between 25°C and 80°C for the screened redox couple combinations - (a) $Fe(CN)_6^{3-/4-}||I_3^-/I^-$, (b) $Cu^{2+/0}||Fe^{2+/3+}$, (c) $Fe^{2+/3+}||$CuHCF, and (d) $Zn(NH_3)_4^{2+}/Zn^0||$NiHCF. Both thermodynamic cycles shift the charging curves higher (a and b) or lower (c and d) than the discharging curves; therefore, net work is produced during these cycles because of the voltage differences. The charge curves are theoretical and exclude some aspects only measurable in a practical system, such as ohmic losses.

compatible range of acidic pH conditions (between 0 and 1.5 due to limitations of the stable pH window of $Fe^{2+/3+}$ ions). This combination of chemicals shows no undesirable effects when working at higher temperatures, but there is the risk of the formation of undesired Cu^+ due to a potential comproportionation reaction,[59] as well as the formation of iron oxide if iron is exposed to the air.[60] However, it shows low cell voltage (0.39V at RT) compared to other selected combinations, which could compromise the energy storage capabilities.

$Fe^{2+/3+}||$CuHCF. This combination also shows a considerable thermal coefficient of -2.12 mV/K and has a higher solubility (1.5M) than the $Fe(CN)_6^{3-/4-}||I_3^-/I^-$ combination. The iron redox couple requires a low pH condition between 0 and 1.5, while CuHCF does not have strict pH value restrictions, showing a wide stable reaction range of 2.5 and 10.2.[61] While studies have been realised for CuHCF being combined with $Cu^{2+/0}$ for low grade heat energy harvesting,[10] $Cu^{2+/3+}||$CuHCF combination could show reduced efficiency in energy generation at higher temperatures. Lee et al. reported a slow decay in coulombic efficiency when operating at temperatures higher than 80°C, leading to poor cyclability.[10] No specific reason for this deterioration was stated and this limits the range of the temperature difference, which is one of the critical aspects for efficient energy harvesting with the TREC (i.e., higher W_{net} for Eq. 1).

A TREC with a $Fe^{2+/3+}||$CuHCF with ClO_4^- anion electrolyte additives demonstrated by Li et al.[23] achieved an impressive α_{cell} of -3.04 mV/K and a 27% efficiency performance referred to the Carnot maximum (ΔT = 50°C), which appears to be the highest TREC reported to date. However, this result was based on a modified electrolyte and was not taken into account in this screening process. Nevertheless, this case is an important study that emphasises a development direction towards electrolyte design.

As shown in Figure 4c, a low OCV (open circuit voltage) is an issue for this combination. We note that the redox chemistry of CuHCF is complex; however, we assume that the *n* value of this pair could be 1 to take a conservative approach.[62] The concentration limit of 1.4M leads to an efficiency estimate, which is over 2.5 times higher than the $Fe(CN)_6^{3-/4-}||I_3^-$ pair, but

Table 2 Specifications of the selected redox couple combinations and theoretical performance metrics. Note that the calculation is based on 99% of the depth of discharging (DoD). The calculation method, assumptions for the calculations, and values for other DoDs are discussed in the ESI.†

Combination	α / mV	$E^0_{25°C}$ / V	Net work / Wh L^{-1}	Q_h / Wh L^{-1}	$\eta_{0.5HR}$ / %	$\eta_{0.7HR}$ / %	$\eta_{0.9HR}$ / %	$\eta_{0.99HR}$ / %	$\eta_{Carnot\ @0.99HR}$ / %
$[Fe(CN)_6]^{3-/4-}||I_3^-/3I^-$	2.46	0.19	1.41	4.66	0.05	0.08	0.24	2.22	13.28
$Fe^{2+/3+}||Cu^{0/2+}$	-2.12	0.47	4.24	14.05	0.14	0.24	0.70	5.83	29.80
$Fe^{2+/3+}||$CuHCF	2.06	0.395	3.89	12.67	0.13	0.22	0.65	5.44	29.90
$[Zn(NH_3)_4]^{2+}/Zn$ || NiHCF	-2.27	1.8	21.72	71.55	0.72	1.18	3.29	16.66	69.55

the single electron charge operation causes $Fe^{2+/3+}$||CuHCF to place third overall in the performance estimation.

$[Zn(NH_3)_4]^{2+}/Zn^0$||NiHCF. The zinc ammonia and nickel hexacyanoferrate combination also displays a significant overall thermal coefficient. Its α_{cell} is the second largest in magnitude at -2.27 mV/K. Studies have shown some positive results for this combination in a TREC application,[9] but have also encountered several flaws in the system. The $[Zn(NH_3)_4]^{2+}/Zn^0$ requires NH_3(aq) to interact with dissolved Zn^{2+} ions in the electrolyte, leading to the diffusion of ammonia through the membrane to the opposite half-cell. Consequently, the α_{cell} magnitude could only be sustained for the first 7 cycles.[9] For these cycles, conversion efficiency was reported at 22.66% (at ΔT = 30°C) of the Carnot maximum with no heat recovery. This compares to our 0.9%HR (heat recovery) value for this pair, which is 19.1%. The difference between these values likely arises from the following two reasons: The heat capacity calculated to be 2.3 J/g by Cheng et al.,[9] while we assume the heat capacities of all cases to be 3.5 J/g which allows us to be conservative with our efficiency results. Secondly, their results were taken from 80-100% SoC, whereas ours is based on a broader SoC range (i.e., a high charging depth of 99%).

The maximum solubility for this pair is 3.33M governed by $ZnSO_4$ dissolved in ammonia solution to form $Zn(NH_3)_4^{2+}$ ions. Also, the full reaction is a two-electron charge transfer, making this combination have the largest charge density (over 15 times the $Fe(CN)_6^{3-/4-}$||I_3^-/I^- pair) and hence yield the highest amount of work. While charge density is only one relevant factor of electrolyte design, it is likely that this disparity would overcome any advantage that $Fe(CN)_6^{3-/4-}$||I_3^- would bring, such as fast charge kinetics. If $Zn(NH_3)_4^{2+}/Zn^0$||NiHCF can be deployed in a stable fashion with good cyclability (*via* using an appropriate membrane), then a highly efficient and practical TREC heat recovery system could be realised. The high output voltage (1.76V) of this pair places it in a good position to yield high power density, currently one of the major shortcomings of TREC systems.

As shown in Table 2, the conversion efficiency for each pair is evaluated at 4 levels of heat recovery. This is to demonstrate the significance of heat management on the overall performance. Maximising alpha and net work are desirable, but the major gains in efficiency are made by re-using the absorbed heat between cycles so that the denominator in Eq. 1 is minimised. As TREC experiments have only existed at a lab scale, it is difficult to use spacious and highly efficient heat exchangers that achieve over 90% of heat recovery efficiency (i.e., 0.9 HR). To bring the TREC to commercial viability, a system-wise optimisation approach must be used that considers the following: charge kinetics of the electrolyte, low electrical loss cell design, and intelligent thermal recovery design. In particular, we emphasise that TREC operates at relatively high temperatures. This may cause a reduction of the cell overpotential, which is not considered in our paper. This advantage, when combined with the promising combinations presented in this paper, can result in a synergistic effect. In this regard, a recent perspective paper on electrochemical kinetic parameters for redox cells by Wang et al.[63] is also highly recommended as a practical guideline.

View Article Online
DOI: 10.1039/D4YA00368C

Conclusions

It can be concluded that there is no perfect combination of chemicals for an optimal TREC redox battery. While the hexacyanoferrate and iodide/polyiodide combination displays the highest thermal coefficient α, it has low OCV and solubility. The combination of $[Zn(NH_3)_4]^{2+}$/Zn and NiHCF has a significantly higher OCV, solubility and a high thermal coefficient but has issues with an ammonia diffusion that would lead to poor cyclability. $Fe^{2+/3+}$ and CuHCF combination also suffers from low OCV issues and has limited efficiency to the full range of low-grade heat. There are still many unexplored combinations, implying that there is untapped potential for further development and higher-performance design.

Selection criterion #2 (i.e., stable reaction behaviour without a precipitation formation or unwanted side reactions at elevated temperatures) has excluded some good candidates for efficient combinations, mainly those including the Br_2/Br^- coup[46] and the all-vanadium TREC RFB studied by Reynard et al.[11] Even though flexibility with this criterion would lead to different results, it is still a valid constraint considering the reliability of the TREC operation.

While the thermal coefficient α is the most determining factor concerning energy generation, it is clearly shown that other properties are also quintessential for the overall efficiency of the whole process, with solubility affecting energy density directly, OCV having a determining effect on power density, and pH stability range of the couples affecting the long-term performance of the cell. A full system approach which minimises losses from all sources is vital to bringing TREC to commercially viable efficiency. The importance of non-chemical factors such as heat recovery cannot be overstated, and this is demonstrated in the analysis (i.e., Table 2).

Concerning Future work and recommendations, even though the overall procedure of the study was done in accordance with high-quality standards, it is purely a literature-driven theoretical approach. As mentioned earlier, electrochemical losses such as overpotentials that occur in real cells were not taken into account. It is worth noting that these may vary considerably depending on the redox couple chosen, the counterion and separator used, as well as possibly varying in their temperature dependence, which could significantly affect the choice of redox couples for a TREC device. Electrochemical kinetics parameters of most of the redox couples here have been studied extensively over the last decades, but the specific electrode, flow field and separator configurations of a device may affect these parameters considerably.

As a relatively unexplored field, every contribution to the knowledge of thermal coefficients of redox couples and their potential applications to the TREC has a huge impact on widening the horizon of understanding of this topic, providing

additional insights, and potentially inspiring further research on the topic.

Author Contributions

José Tomás Bórquez Maldifassi: Writing - original draft, Writing – review & editing, Visualization, Data curation, Formal analysis; **Joseph B. Russell**: Visualization, Writing – review & editing, Formal analysis, **Jungmyung Kim**: Writing – review & editing; **Edward Brightman** Writing - review & editing; **Xiangjie Chen**: Writing - review & editing; **Dowon Bae**: Conceptualization, Methodology, Visualization, Writing – review & editing, Resources, Supervision, Funding acquisition.

Conflicts of interest

There are no conflicts to declare.

Acknowledgements

J.T.B.M. thanks to Tasneema Akhtar, Oismita Mitra, and Elpida Gkika for their help in fundamental concept learning of redox chemistry. D.B., J.K., and E.B. acknowledge the Engineering and Physical Sciences Research Council of the UK (EPSRC; grant no. EP/X015920/1 and EP/X015920/2) for the financial support. D.B., J.K., and J.B.R. also thank Dr Stuart Robertson (The University of Strathclyde) for his help.

Notes and references

1 M. Luberti, R. Gowans, P. Finn and G. Santori, An estimate of the ultralow waste heat available in the European Union, *Energy*, 2022, **238**, 121967.

2 C. Gao, S. W. Lee and Y. Yang, Thermally Regenerative Electrochemical Cycle for Low-Grade Heat Harvesting, *ACS Energy Lett*, 2017, **2**, 2326–2334.

3 D. Bae and A. Bentien, Take it to the Carnot limit: Perspectives and thermodynamics of dual-cell electrochemical heat engines, *Energy Convers Manag*, 2022, **271**, 116315.

4 J. Bleeker, S. Reichert, J. Veerman and D. A. Vermaas, Thermo-electrochemical redox flow cycle for continuous conversion of low-grade waste heat to power, *Sci Rep*, 2022, **12**, 17993.

5 D. Bae, G. M. Faasse and W. A. Smith, Hidden figures of photo-charging: a thermo-electrochemical approach for a solar-rechargeable redox flow cell system, *Sustain Energy Fuels*, 2020, **4**, 2650–2655.

6 H. Zhang, Y. Cheng, D. G. Lek, T. Liu, F. Lin, W. Luo, S. Huang, M. Gao, X. Wang, Y. Zhi and Q. Wang, Membrane-free redox flow cell based on thermally regenerative electrochemical cycle for concurrent electricity storage, cooling and waste heat harnessing of perovskite solar cells, *J Power Sources*, 2022, **548**, 232081.

7 X. Wang, Y. T. Huang, C. Liu, K. Mu, K. H. Li, S. Wang, Y. Yang, L. Wang, C. H. Su and S. P. Feng, Direct thermal charging cell for converting low-grade heat to electricity, *Nat Commun*, 2019, **10**, 1–8.

8 Y. Yang, J. Loomis, H. Ghasemi, S. W. Lee, Y. J. Wang, Y. Cui and G. Chen, Membrane-free battery for harvesting low-grade thermal energy, *Nano Lett*, 2014, **14**, 6578–6583.

9 C. Cheng, S. Wang, P. Tan, Y. Dai, J. Yu, R. Cheng, S. P. Feng and M. Ni, Insights into the Thermopower of Thermally Regenerative Electrochemical Cycle for Low Grade Heat Harvesting, *ACS Energy Lett*, 2021, **6**, 329–336.

10 S. W. Lee, Y. Yang, H. W. Lee, H. Ghasemi, D. Kraemer, G. Chen and Y. Cui, An electrochemical system for efficiently harvesting low-grade heat energy, *Nat Commun*, 2014, **5**, 3942.

11 D. Reynard, C. R. Dennison, A. Battistel and H. H. Girault, Efficiency improvement of an all-vanadium redox flow battery by harvesting low-grade heat, *J Power Sources*, 2018, **390**, 30–37.

12 Y. Liang, J. Ka-Ho Hui, M. A. Morikawa, H. Inoue, T. Yamada and N. Kimizuka, High Positive Seebeck Coefficient of Aqueous I-/I3- Thermocells Based on Host-Guest Interactions and LCST Behavior of PEGylated α-Cyclodextrin, *ACS Appl Energy Mater*, 2021, **4**, 5326–5331.

13 K. Shindo, M. Arakawa and T. Hirai, Effect of non-graphitized carbon electrodes on the

View Article Online DOI: 10.1039/D4YA00368C

electrochemical characteristics of a thermocell with a Br2/Br- redox couple, *J Power Sources*, 1998, **70**, 228–234.

14 J. H. Kim, J. H. Lee, R. R. Palem, M. S. Suh, H. H. Lee and T. J. Kang, Iron (II/III) perchlorate electrolytes for electrochemically harvesting low-grade thermal energy, *Sci Rep*, 2019, **9**, 8706.

15 A. Abdollahipour and H. Sayyaadi, A review of thermally regenerative electrochemical systems for power generation and refrigeration applications, *Appl Therm Eng*, 2021, **187**, 116576.

16 Y. Yang, S. W. Lee, H. Ghasemi, J. Loomis, X. Li, D. Kraemer, G. Zheng, Y. Cui and G. Chen, Charging-free electrochemical system for harvesting low-grade thermal energy, *Proc Natl Acad Sci U S A*, 2014, **111**, 17011–17016.

17 P. Loktionov, D. Konev, R. Pichugov and A. Antipov, Electrochemical heat engine based on neutralization flow battery for continuous low-grade heat harvesting, *Energy Convers Manag*, 2024, **299**, 117830.

18 A. Rajan, I. S. McKay and S. K. Yee, Continuous electrochemical refrigeration based on the Brayton cycle, *Nat Energy*, 2022, **7**, 320–328.

19 R. Chen, S. Deng, J. Zhang, L. Zhao, W. Xu and R. Zhao, Exploring a novel route for low-grade heat harvesting: Electrochemical Brayton cycle, *Renewable and Sustainable Energy Reviews*, 2023, **183**, 113475.

20 R. H. Hammond and W. M. Risen, An electrochemical heat engine for direct solar energy conversion, *Solar Energy*, 1979, **23**, 443–449.

21 J. Duan, G. Feng, B. Yu, J. Li, M. Chen, P. Yang, J. Feng, K. Liu and J. Zhou, Aqueous thermogalvanic cells with a high Seebeck coefficient for low-grade heat harvest, *Nature Communications 2018 9:1*, 2018, **9**, 1–8.

22 J. Li, X. Li, D. Lee, J. Yun, A. Wu, C. Jiang and S. W. Lee, Engineering of Solvation Entropy by Poly(4-styrenesulfonic acid) Additive in an Aqueous Electrochemical System for Enhanced Low-Grade Heat Harvesting, *Nano Lett*, 2023, **23**, 6164–6170.

23 X. Li, A. Wu, J. Li, Z. Li, D. Lee and S. W. Lee, Anion Effects on Thermopower of Electrochemical Systems for Low-Grade Heat Harvesting, *ACS Energy Lett*, 2023, **8**, 4061–4068.

24 F. Pan and Q. Wang, Redox species of redox flow batteries: A review, *Molecules*, 2015, **20**, 20499–20517.

25 R. Duke, V. Bhat, P. Sornberger, S. A. Odom and C. Risko, Towards a comprehensive data infrastructure for redox-active organic molecules targeting nonaqueous redox flow batteries, *Digital Discovery*, 2023, **2**, 1152–1162.

26 E. Sorkun, Q. Zhang, A. Khetan, M. C. Sorkun and S. Er, RedDB, a computational database of electroactive molecules for aqueous redox flow batteries, *Sci Data*, 2022, **9**, 718.

27 M. A. Blommaert, D. Aili, R. A. Tufa, Q. Li, W. A. Smith and D. A. Vermaas, Insights and Challenges for Applying Bipolar Membranes in Advanced Electrochemical Energy Systems, *ACS Energy Lett*, 2021, **6**, 2539–2548.

28 H. H. Huang, The Eh-pH diagram and its advances, *Metals (Basel)*, 2016, **6**, 23.

29 D. Reber, J. R. Thurston, M. Becker and M. P. Marshak, Stability of highly soluble ferrocyanides at neutral pH for energy-dense flow batteries, *Cell Rep Phys Sci*, 2023, **4**, 101215.

30 S. Titretir, G. Erdogu and A. Karagözler, Determination of iodide ions at poly(3-methylthiophene)-modified electrode by differential pulse stripping voltammetry, *Journal of analytic chemistry*, 2006, **61**, 592–595.

31 S. Osborn, The University of Arizona, 2010.

32 M. Endo, Y. Yamagishi and M. Inagaki, Thermocell with graphite fiber-bromine intercalation compounds, *Synth Met*, 1983, **7**, 203–209.

33 M. Mohammad, M. Tariq and M. T. Soomro, 'Long-life' atom-free radical: Generation and reactions of bromine atom-free radical, *Collect Czechoslov Chem Commun*, 2010, **75**, 1061–1074.

34 German Federal Ministry for Economic Cooperation and Development, Ed., in *Environmental Handbook: Documentation on Monitoring and Evaluating Environmental Impacts*, 1996.

35 N. Takeno, *Atlas of Eh-pH diagrams: Intercomparison of thermodynamic databases*, 2005.

36 H. Zhang, F. Zhang, J. Yu, M. Zhou, W. Luo, Y. M. Lee, M. Si and Q. Wang, Redox Targeting-Based Thermally Regenerative Electrochemical Cycle Flow Cell for Enhanced Low-Grade Heat Harnessing, *Advanced Materials*, 2020, **33**, 2006234.

37 LENNTECH B.V., Zinc in water (Zn + H2O), https://www.lenntech.com/periodic/water/zinc/zinc-and-water.htm, (accessed 14 September 2024).

38 Y. Yu, J. Xie, H. Zhang, R. Qin, X. Liu and X. Lu, High-Voltage Rechargeable Aqueous Zinc-Based Batteries: Latest Progress and Future Perspectives, *Small Science*, 2021, **1**, 2000066.

39 W. M. Haynes, *CRC Handbook of Chemistry and Physics, 95th Edition, 2014-2015*, CRC Press, 95th edn., 2014.

40 M. Hans, S. Mathews, F. Mücklich and M. Solioz, Physicochemical properties of copper important for its antibacterial activity and development of a unified model, *Biointerphases*, 2016, **11**, 018902.

41 F. Zhang, N. LaBarge, W. Yang, J. Liu and B. E. Logan, Enhancing Low-Grade Thermal Energy Recovery in a Thermally Regenerative Ammonia Battery Using Elevated Temperatures, *ChemSusChem*, 2015, **8**, 1043–1048.

42 J. L. Anderson and I. Shain, Cyclic Voltammetric Studies of the pH Dependence of Copper(II) Reduction in Acidic Aqueous Nitrate and Perchlorate Solutions, *Anal Chem*, 1976, **48**, 1274–1282.

43 L. Velásquez-Yévenes and R. Ram, The aqueous chemistry of the copper-ammonia system and its implications for the sustainable recovery of copper, *Clean Eng Technol*, 2022, **9**, 100515.

44 D. Grujicic and B. Pesic, Reaction and nucleation mechanisms of copper electrodeposition from ammoniacal solutions on vitreous carbon, *Electrochim Acta*, 2005, **50**, 4426–4443.

45 J. Pan, M. Huang, X. Li, S. Wang, W. Li, T. Ma, X. Xie and V. Ramani, The performance of all vanadium redox flow batteries at below-ambient temperatures, *Energy*, 2016, **107**, 784–790.

46 M. Lee, X. Ding, S. Banerjee, F. Krause, V. Smirnov, O. Astakhov, T. Merdzhanova, B. Klingebiel, T. Kirchartz, F. Finger, U. Rau and S. Haas, Bifunctional CoFeVOx Catalyst for Solar Water Splitting by using Multijunction and Heterojunction Silicon Solar Cells, *Adv Mater Technol*, 2020, **5**, 2000592.

47 A. J. Bard, R. Parsons and J. Jordan, *Standard Potentials in Aqueous Solution*, 2017.

48 J. Jiang, H. Tian, X. He, Q. Zeng, Y. Niu, T. Zhou, Y. Yang and C. Wang, A CoHCF system with enhanced energy conversion efficiency for low-grade heat harvesting, *J Mater Chem A Mater*, 2019, **7**, 23862–23867.

49 Sigma Aldrich, Solubility Table of Compounds in Water at Temperature, https://www.sigmaaldrich.com/GB/en/support/calculators-and-apps/solubility-table-compounds-water-temperature, (accessed 16 September 2024).

50 A. Holland, R. D. Mckerracher, A. Cruden and R. G. A. Wills, An aluminium battery operating with an aqueous electrolyte, *J Appl Electrochem*, 2018, **48**, 243–250.

51 Y. Fukuzumi, Y. Hinuma and Y. Moritomo, Thermal coefficient of redox potential of alkali metals, *J Physical Soc Japan*, 2018, **87**, 055001.

52 P. Jakhar, S. Mayoorika and V. Singh, Investigation of dopant effect on the electrochemical performance of 1-D polypyrrole nanofibers based glucose biosensor, *Journal of Materials Science: Materials in Electronics*, 2019, **30**, 3563–3573.

53 K. Shindo, M. Arakawa and T. Hirai, Influence of electrode materials on open-circuit voltage profiles with a temperature difference for a thermocell using a Br2/Br--redox reaction, *J Power Sources*, 2002, **110**, 46–51.

54 D. Huo, H. Tian, G. Shu and W. Wang, Progress and prospects for low-grade heat recovery electrochemical technologies, *Sustainable Energy Technologies and Assessments*, 2022, **49**, 101802.

55 D. Huo, H. Tian, W. Wang and G. Shu, Na/K mixed electrolyte for high power density and heat-to-electricity conversion efficiency low-grade heat harvesting system, *Mater Today Nano*, 2022, **18**, 100206.

56 C. Gao, Y. Liu, B. Chen, J. Yun, E. Feng, Y. Kim, M. Kim, A. Choi, H. W. Lee and S. W. Lee, Efficient Low-Grade Heat Harvesting Enabled by Tuning the Hydration Entropy in an Electrochemical System, *Advanced Materials*, 2021, **33**, 1–9.

57 X. Qian, J. Shin, Y. Tu, J. H. Zhang and G. Chen, Thermally regenerative electrochemically cycled flow batteries with pH neutral electrolytes for harvesting low-grade heat, *Physical Chemistry Chemical Physics*, 2021, **23**, 22501–22514.

58 G. M. Weng, Z. Li, G. Cong, Y. Zhou and Y. C. Lu, Unlocking the capacity of iodide for high-energy-density zinc/polyiodide and lithium/polyiodide redox flow batteries, *Energy Environ Sci*, 2017, **10**, 735–741.

59 W. Dirk, L. Sanz, C. Arbizzani and L. Murtomäki, Performance improvements for the all-copper redox flow battery: Membranes, electrodes, and electrolytes, *Energy Reports*, 2022, **8**, 8690–8700.

60 P. S. Borchers, M. Strumpf, C. Friebe, I. Nischang, M. D. Hager, J. Elbert and U. S. Schubert, Aqueous Redox Flow Battery Suitable for High Temperature Applications Based on a Tailor-Made Ferrocene Copolymer, *Adv Energy Mater*, 2020, **10**, 2001825.

61 L. Shi, E. Newcomer, M. Son, V. Pothanamkandathil, C. A. Gorski, A. Galal and B. E. Logan, Metal-Ion Depletion Impacts the Stability and Performance of Battery Electrode Deionization over Multiple Cycles, *Environ Sci Technol*, 2021, **55**, 5412–5421.

62 Z. Song, W. Liu, X. Wei, Q. Zhou, H. Liu, Z. Zhang, G. Liu and Z. Zhao, Charge storage mechanism of copper hexacyanoferrate nanocubes for supercapacitors, *Chinese Chemical Letters*, 2020, **31**, 1213–1216.

63 H. Wang, S. Y. Sayed, E. J. Luber, B. C. Olsen, S. M. Shirurkar, S. Venkatakrishnan, U. M. Tefashe, A. K. Farquhar, E. S. Smotkin, R. L. McCreery and J. M. Buriak, Redox Flow Batteries: How to Determine Electrochemical Kinetic Parameters, *ACS Nano*, 2020, **14**, 2575–2584.

View Article Online
DOI: 10.1039/D4YA00368C

View Article Online
DOI: 10.1039/D4YA00368C

Data availability statements

The data that support the calculation method of this study and basic assumptions made for the calculations have been included as part of the Supplementary Information.

Also, tabularized values of redox couples' solubilities and cell voltages under standard conditions are publicly available in Loughborough University Research Repository, ttps://doi.org/10.17028/rd.lboro.25999504.